heritage

IMPACT FACTOR 1.7

CITESCORE 2.8

Article

The High Potential of Micro-Magnetic Resonance Imaging for the Identification of Archaeological Reeds: The Case Study of Tutankhamun

Claudia Moricca, Valeria Stagno, Nagmeldeen Morshed Hamza, Gabriele Favero, Laura Sadori and Silvia Capuani

Special Issue

Non-invasive Technologies Applied in Cultural Heritage

Edited by

Dr. Silvano Mignardi, Dr. Wenke Zhao, Dr. Laura Medeghini, Dr. Melania Di Fazio and Laura Calzolari

MDPI

https://doi.org/10.3390/heritage6110375

heritage

MDPI

Article

The High Potential of Micro-Magnetic Resonance Imaging for the Identification of Archaeological Reeds: The Case Study of Tutankhamun

Claudia Moricca [1], Valeria Stagno [2,*], Nagmeldeen Morshed Hamza [1,3,4], Gabriele Favero [1], Laura Sadori [1,*] and Silvia Capuani [2]

[1] Department of Environmental Biology, Sapienza University of Rome, Piazzale Aldo Moro 5, 00185 Rome, Italy; claudia.moricca@uniroma1.it (C.M.); nagmeldeenmorshed.hamza@uniroma1.it (N.M.H.); gabriele.favero@uniroma1.it (G.F.)
[2] National Research Council—Institute for Complex Systems (CNR-ISC) c/o Department of Physics, Sapienza University of Rome, Piazzale Aldo Moro 5, 00185 Rome, Italy; silvia.capuani@isc.cnr.it
[3] Department of Earth Sciences, Sapienza University of Rome, Piazzale Aldo Moro 5, 00185 Rome, Italy
[4] Grand Egyptian Museum, Conservation Center, Al Remaya Square, Al Haram, Giza 3513204, Egypt
* Correspondence: valeria.stagno@uniroma1.it (V.S.); laura.sadori@uniroma1.it (L.S.)

Abstract: This study explores the potential of micro-magnetic resonance imaging (μ-MRI) for identifying archaeological reeds found in the tomb of Tutankhamun. Reed plants had various historical uses in the past, with ancient Egyptians extensively employing them for crafting a wide range of items. The distinct cross-sectional characteristics of *Arundo donax* (giant reed) and *Phragmites australis* (common reed) are observed and described via optical microscopy and μ-MRI in this study. While optical microscopy offers higher resolution, μ-MRI provides advantages for studying archaeobotanical specimens, as it eliminates the need for mechanical sectioning and potentially damaging fragile samples. The application of μ-MRI on a selected archaeological reed allowed us to identify it as *Phragmites australis*, showing that μ-MRI can yield clear images, maintaining the integrity of the sample. In contrast, diagnostic features appeared greatly deformed on the thin section observed via optical microscopy. Despite the limitations related to the sample size and the need for sample soaking, μ-MRI presents a valuable tool for analyzing archaeological remains in the field of cultural heritage, with the potential for broader applications. Overall, this study contributes to expanding the toolkit available to researchers studying plant remains, providing insights into reed identification and preservation in archaeological contexts.

Keywords: optical microscopy; wood imaging; reed anatomy; ancient Egypt; archaeobotany; desiccated plant remains; diagnostic technique

check for updates

Citation: Moricca, C.; Stagno, V.; Hamza, N.M.; Favero, G.; Sadori, L.; Capuani, S. The High Potential of Micro-Magnetic Resonance Imaging for the Identification of Archaeological Reeds: The Case Study of Tutankhamun. *Heritage* **2023**, *6*, 7170–7180. https://doi.org/10.3390/heritage6110375

Academic Editor: Diego Tamburini

Received: 23 October 2023
Revised: 14 November 2023
Accepted: 14 November 2023
Published: 16 November 2023

Copyright: © 2023 by the authors. Licensee MDPI, Basel, Switzerland. This article is an open access article distributed under the terms and conditions of the Creative Commons Attribution (CC BY) license (https://creativecommons.org/licenses/by/4.0/).

1. Introduction

Reeds are herbaceous, rhizomatous, perennial plants belonging to the Poaceae family. They typically grow along rivers or on the edges of ponds in shallow water [1]. They are characterized by robust and lightweight cylindrical stems. The mechanical properties of the fibers they are composed of make reeds strong and elastic [2]. For this reason, reeds have been used for various purposes throughout human history, for example, in the construction of huts [3], rafts and boats [4], tools, and common objects [5]. Reeds have played an important role in the development of music and continue to be used to produce woodwind instruments such as clarinets [6] and the Japanese hichikiri [7]. While it is difficult to estimate when reeds were first used for this purpose, single-toned pipes made of bone (a material less subjected to biodeterioration) have been attested since the early Stone Age [8].

Archaeobotany, the study of plant remains found in archaeological contexts, is of great help in reconstructing past human-plant relationships. Humans have always exploited natural resources not only to obtain food but also to create raw materials such as ropes, fabric, and wood. They have shaped and modified the surrounding environment by domesticating crop plants using land for pasture and agriculture, generally leading to a decline in forest cover [9]. Plant remains can be classified based on size, with macro-remains (e.g., seeds, fruits, and wood) being visible to the naked eye. Their preservation in archaeological layers can occur in different modalities, which include charring and waterlogging [10]. The arid climate, which characterizes Egypt, has favored the preservation of numerous plant materials by desiccation, leaving direct evidence of the past application of reeds. In the Predynastic and Pharaonic periods, *Phragmites australis* (Cav.) Steud. (common reed), *Arundo donax* L. (giant reed), and *Saccharum spontaneum* L. (wild sugarcane) were used to make baskets, ropes, nets, sandals, fishing rods, walking sticks, arrows, and other objects [11,12]. Writing tools were also obtained from culms, which were cut obliquely and split like a quill pen. Culms were not the only plant part being used, as leaves found an application for making mats and wrapping the bodies of the deceased, while rhizomes were used in traditional medicine due to their diuretic and diaphoretic properties [9]. Amongst the three mentioned species, *Phragmites australis* is reported to have been used the most in the Predynastic and Pharaonic periods in Ancient Egypt [11].

While material evidence already provides much information about the use of reeds by ancient Egyptians, iconography can provide extra insight. *Phragmites* were used as a hieroglyphic sign [13] and are illustrated on wall paintings, such as those of the Tomb of Puyemre, the Temple of King Sethos I at Abydos [14], and the temple of Ramses III (20th Dynasty) in Medinet Habu [15]. In contrast, the mural paintings in the tomb of Nakht (18th Dynasty) are believed to depict *Arundo* along with papyrus [14].

In this context, identifying the reed plants preserved in Egyptian tombs is of particular interest, allowing us to assess plant availability and selection of raw materials. An interesting case study is represented by the famous tomb of Tutankhamun (1334–1325 BC—18th Dynasty), discovered by the archaeologist Howard Carter in 1922, where several reed objects were recovered. These include reed arrows (inventory numbers 046a, 048y, and 050yy), baskets (042, 093, 097, 117a, 129, and 146), a kohl tube (044y), a reed pad (052), sandals (094a, 104b), a tray with partitions (119), a cane decorated with gold at both ends (229), a bundle of reeds (249), a torch upon sun-dried brick (263), a pen case (271e), two statuettes of the King upon a float, and a mat (442d) [16]. Reed fragments were also recently recovered from a wooden box containing all the remains swept from the tomb surfaces after all the other objects were photographed (Figure 1). The box was closed in 1933 and stored in the Egyptian Museum in Cairo until 2017. In 2018, it was moved to the Grand Egyptian Museum, where its contents were subjected to scientific analyses [17,18].

Figure 1. Some of the reed fragments found in the wooden box containing the remains swept from the surfaces of Tutankhamun's tomb.

Reed Anatomy and Its Study

Reeds are monocotyledons, flowering plants whose seed germinates from one embryonic leaf. This means that, unlike wood, they lack the tissues that form new (secondary) growth in thickness, as well as the vascular cambium and a long-lived primary root [19]. The different layers with different functions can be observed by looking at the stem cross-section, which can be used to identify the plant taxon. Reeds present a circular cross-section outline [20], but a square or triangular outline can be of diagnostic value for specific plant taxa, such as Lamiaceae or *Carex* [19].

The outermost layer is called the epidermis and can comprise one or more layers. This is followed by the hypodermis, often defined as absent if it does not show significant differences from the adjacent cortical layer, the cortex. The latter can be very narrow or wide and multi-layered. It is delimited on the inner side by the endodermis and sometimes contains some vascular bundles. Vascular bundles, the conducting vessels of the plant, are usually embedded in the sclerenchyma. They can be surrounded by a cap of fibers [19]. Reed stems have vascular bundles with two metaxylem vessels and one phloem pole [21].

Unlike wood, whose diagnostic features are observed along three anatomical sections (transverse/cross, tangential, and radial), reed stem identification is performed by solely observing the cross-section [21]. This is typically performed via optical microscopy (e.g., [21]), although scanning electron microscopy (SEM) can also be used (e.g., [22]). Anatomical differences between *Arundo donax* and *Phragmites australis* stem anatomy are slight [22]. For this reason, discerning between the two in archaeological contexts is problematic (e.g., [23,24]).

A recent advance in the study of plant stem anatomy is represented using micro-magnetic resonance imaging (μ-MRI), based on the analysis of magnetic properties of hydrogen nuclei and the resonance phenomenon [25]. μ-MRI allows the observation of the internal anatomy of biological materials and tissues through images representative of the spatial distribution of mobile protons (mainly from water). μ-MRI is a multi-parametric investigation. It provides superimposed anatomical information on chemical–physical and physiological features obtained using MR images "weighted" with different MRI parameters, such as the relaxation times T_1, T_2, and T_2* of water protons surrounding the environment [26]. The μ-MRI technique allows the acquisition of an infinite number of images by virtually slicing the sample with an extremely variable orientation and currently reaches an in-plane resolution of 8×8 μm^2 [25]. This method has already been used to investigate archaeological wood [25,27–29], demonstrating the advantage of not needing to mechanically section the sample, in contrast to the transmitted light microscopy technique. It was also tested against the latter technique, proving to be a promising and complementary wood diagnostic method [25]. In this study, we aim to test, for the first time, the potential of μ-MRI for studying the anatomy of monocotyledon stems. While it is important from a methodological point of view, our study also contributes to the understanding of plant exploitation in the 18th Dynasty of Egypt, shedding some light on the mystery of pharaoh Tutankhamun. In fact, in Germer's study of plant remains from the tomb of the king [30], numerous reed artifacts were identified as being made of either *Arundo donax* or *Phragmites australis*.

2. Materials and Methods

2.1. Sample Preparation

A total of three reed samples were analyzed in the present work. The first two fragments are modern reference samples of reed stems (*Arundo donax* and *Phragmites australis*) collected along the shores of the Aniene River, in Rome (RM), outside the *Grande Raccordo Anulare*, of about 1.5 cm in height and 2 mm in thickness. The third sample is an archaeological fragment of an unknown reed (size ca. 1×0.5 cm). *A. donax* and *P. australis* were selected because, unlike *Saccharum spontaneum*, also used in ancient Egypt [31], they have a hollow stem [21,32]. The third sample (size ca. 1×0.5 cm) was found inside

the box containing the sweepings from the tomb of Tutankhamun and had not been previously identified.

A stereomicroscopic observation was performed prior to this study in an attempt to identify the sample without soaking or cutting. However, it was inconclusive for the identification of the specimen. The size of modern samples was chosen to fit the NMR capillary tube, which has a diameter of 10 mm. The sample preparation (of both archaeological and reference specimens) consisted of soaking the fragments in distilled water until they sank, indicating their complete saturation. This was necessary to exploit most of the potential offered by NMR by increasing the signal-to-noise ratio (SNR) to improve the MR image quality. Sample soaking was also essential for preparing thin sections to be observed via optical microscopy.

2.2. Optical Microscopy (OM)

Thin cross-sections of the soaked samples were later obtained through mechanical cutting using a razor blade, which was used to cut the samples perpendicular to the growth direction of each reed. These sections were then mounted on a slide and observed using a transmitted light Leica DM750 microscope (magnification: 40×, 100×, and 200×). A Leica ICC50W camera and the Leica Application Suite (version 4.13.0) were then used to acquire pictures.

2.3. Micro-Magnetic Resonance Imaging (µ-MRI)

MR images were obtained by virtually cutting the waterlogged samples acquired using a Bruker Avance-400 spectrometer operating at 9.4 T with a 10 mm micro-imaging probe equipped with a high-performance and high-strength magnetic field gradient unit characterized by a maximum gradient strength of 1200 mT/m and a rise time of 100 µ. A FLASH-type sequence, with parameters optimized for the different samples, was used to obtain T_2*-weighted images. All the parameters used, such as echo time (TE), repetition time (TR), in-plane resolution (R), number of slices (N° slices), slice thickness (STK), number of scans (NS), matrix size (MTX), field of view (FOV), and acquisition time (AT) are reported in Table 1.

Table 1. Optimized µ-MRI acquisition parameters.

Parameters	Archaeological Unknown Reed	*Arundo donax*	*Phragmites australis*
N° slices	4	3	4
TR (ms)	450	800	1000
TE (ms)	4.7	2.8	3.0
STK (µm)	500	500	500
FOV (cm)	0.85	0.90	0.95
MTX (mm^2)	512	512	512
NS	128	256	128
AT (h)	8	29	18
R (μm^2)	17 × 17	17 × 17	18 × 18

3. Results

3.1. Arundo donax

A thin section of *Arundo donax* observed via optical microscopy is shown in Figure 2a, allowing us to assess the stem anatomy of the plant. A rather thick epidermis (outer layer) can be observed. This is followed by two layers of small cells and eight layers of larger cells. These are all thick-walled and rounded. No vascular bundles can be observed within the cortex. The sclerenchyma cylinder has a thickness of 6–8 cells, and vascular bundles are interspersed throughout. The vascular bundles are comprised of two very large metaxylem

vessels, a protophloem of approximately the same size as the metaxylem vessels, and one or two rather thick-walled, small vessels. Vascular bundles are surrounded by sclerenchyma sheaths, which are thicker on the side of the protophloem and often discontinuous in the proximity of the sieve tubes. These characteristics are in accordance with the description provided by Schweingruber [21].

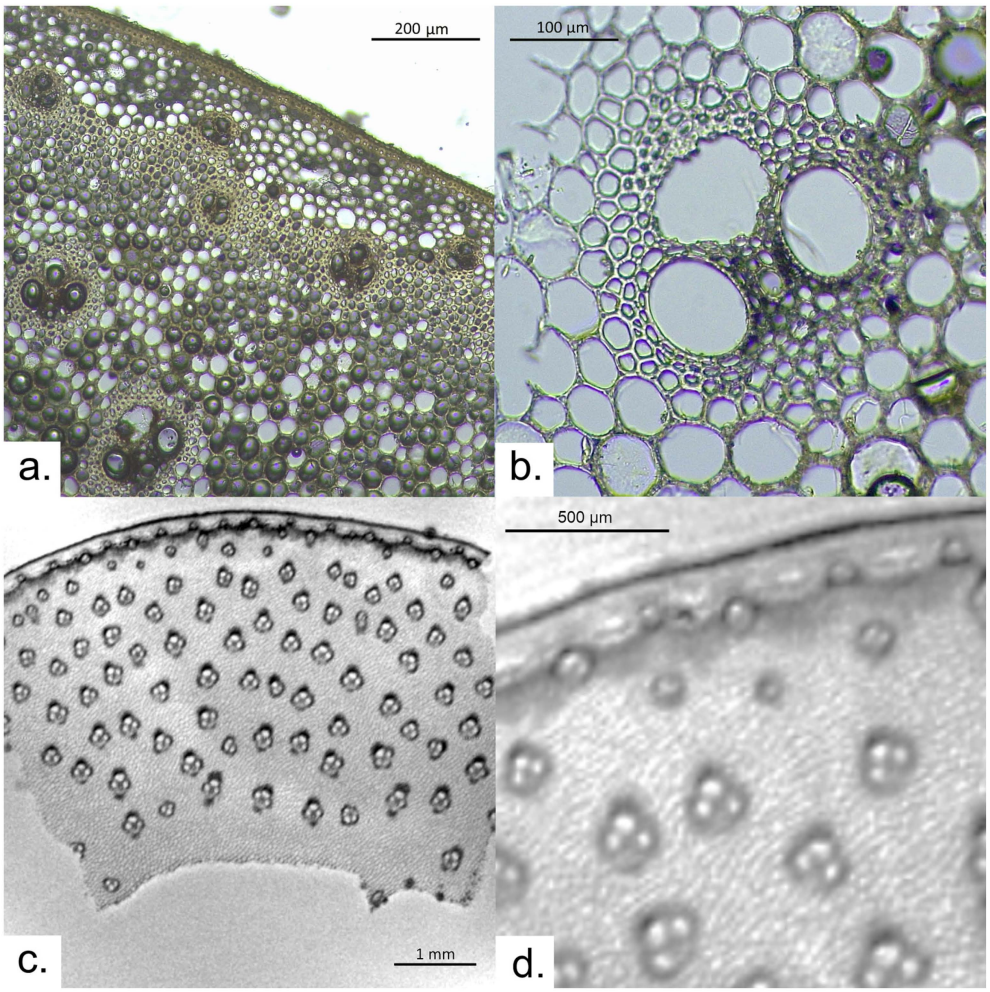

Figure 2. *Arundo donax*: (**a**) thin section observed via optical microscopy; (**b**) detail on a vascular bundle observed via OM; (**c**) µ-MRI image of a sample slice; and (**d**) a zoomed part of the µ-MRI image.

The T_2*-weighted MR image (Figure 2b) makes it possible to see the entire section, 4.3 mm thick, from the epidermis to the inner surface. Most of the features can be observed, with different contrasts. Indeed, T_2*-weighted images are characterized by a contrast that depends both on the T_2 value and the differences in the magnetic susceptibility between different tissues, which highlights the paramagnetic impurities that may be present in the sample [25]. Although the resolution—lower than in optical microscopy—does not allow for the counting of the number of cells making up each layer, the rather thick epidermis is clearly visible. The thin layer made of rather dark voxels suggests the presence of layers of small cells, with very small lumens characterized by very short T_2. This area is followed by a thicker layer of larger cells, characterized by voxels that are lighter due to their bigger lumen size, which causes a slower T_2 relaxation. This is caused by filling the elongated cells with water. Vascular bundles can be observed in the sclerenchyma cylinder, while eight rows of vascular bundles are visible in the remaining part of the cross-section (density ~389 vascular bundles/cm^2). Vascular bundles appear to be slightly taller than wide and have a width of approximately 250 µm. The MR image also allows us to identify them as being composed of three large cavities (two metaxylem vessels and

the protophloem). In some of them, the presence of one or two sieve tubes can also be noticed. The sclerenchyma surrounding the vascular bundles provides dark voxels in the proximity of the protophloem, caused by the difference in the magnetic susceptibility in the different tissues. Moreover, the sclerenchyma cells have a smaller lumen, leading to water being more hindered and defined by shorter T_2 values compared to the water stored in the metaxylem vessels. Finally, in the MR image, it is possible to see the inner surface of the stem.

3.2. *Phragmites australis*

A thin section of *Phragmites australis* observed using optical microscopy is pictured in Figure 3a, making it possible to describe its stem anatomy. In this case, the epidermis is of medium thickness and is followed inwards by 3–4 layers of very thick-walled small cells. No vascular bundles are embedded in the cortex, while they can be observed in the sclerenchyma cylinder. The vascular bundles resemble those of *Arundo donax*, except the sclerenchyma sheaths are thinner. This description is in accordance with that provided by Schweingruber [21].

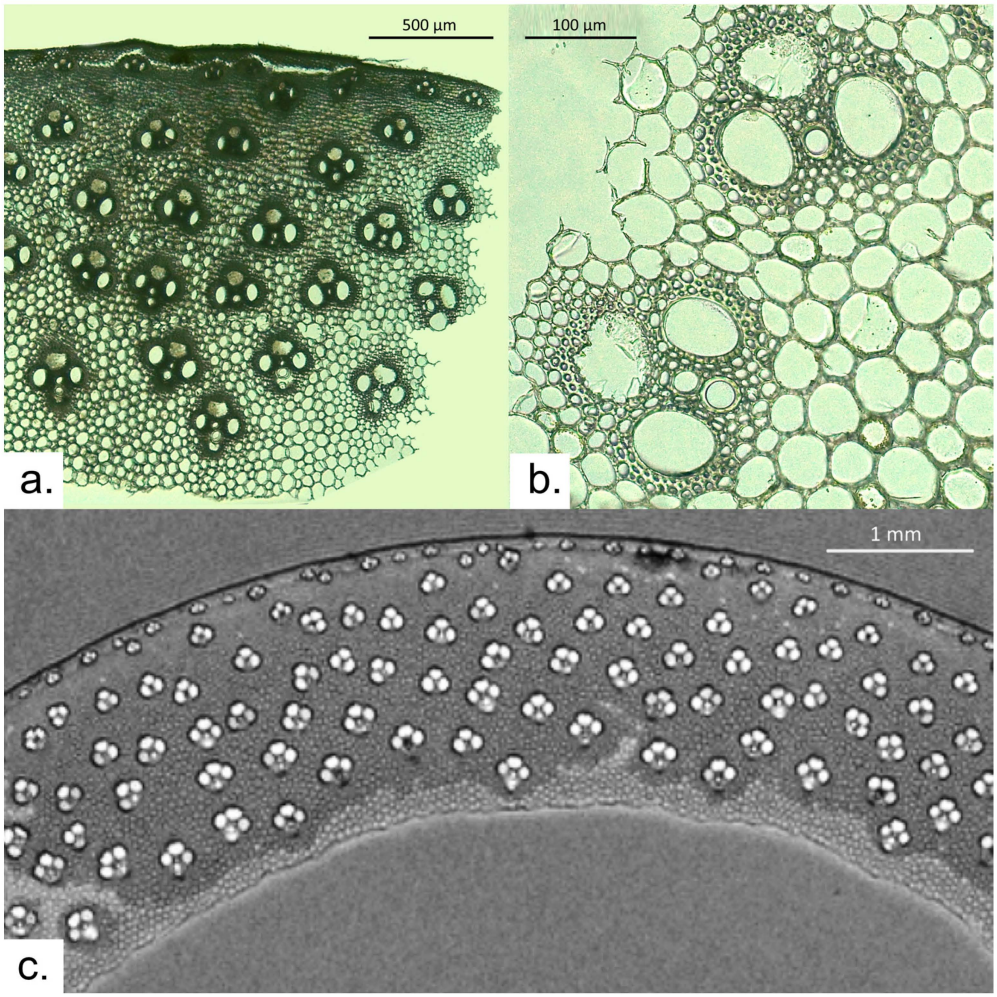

Figure 3. *Phragmites australis*: (**a**) thin section observed via optical microscopy; (**b**) close-up on two vascular bundles observed via OM; and (**c**) µ-MRI image of a sample slice.

The T_2*-weighted MR image of *P. australis* (Figure 3b) makes it possible to appreciate most stem features with different contrasts. The thickness of the stem is ca. 1.8 mm. The epidermis, slightly thinner than that of *A. donax*, is characterized by very dark voxels due to the presence of cells with a very small lumen. This layer is followed by a thin cortex. Vascular bundles (with light voxels due to the bigger diameter of the cells they are made of)

are visible in the sclerenchyma, while five other rows can be observed in the remaining part of the cross-section (density ~900 vascular bundles/cm^2). Vascular bundles appear to be slightly wider than tall and have a width of ca. 200 µm. They are comprised of three large cells (two metaxylem vessels and the protophloem). The vascular bundles are made up of two very large metaxylem vessels, a protophloem of approximately the same size as the metaxylem vessels, and one or two rather thick-walled, small vessels. In some cases, it is also possible to appreciate the presence of one or two smaller cells, the sieve tubes. A thin layer of sclerenchyma surrounding the vascular bundles displays darker voxels due to the difference in the magnetic susceptibility between different tissues. Moreover, sclerenchyma is also characterized by a shorter T_2 due to the smaller lumen of its cells. The MR image also shows the inner surface of the stem. The cells that make it up have lighter voxels due to the thinner-walled cells that make it up.

3.3. Archaeological Sample

The thin section of the archaeological sample (Figure 4a) allows us to observe an outer layer composed of approximately six rows of cells with a very small lumen. Another feature that can be seen is vascular bundles. These appear deeply deformed. It is possible to describe only one of them, at a higher magnification (Figure 4b), as composed of three large cavities and a sieve tube. The vascular bundle is surrounded by sclerenchymatous fibers.

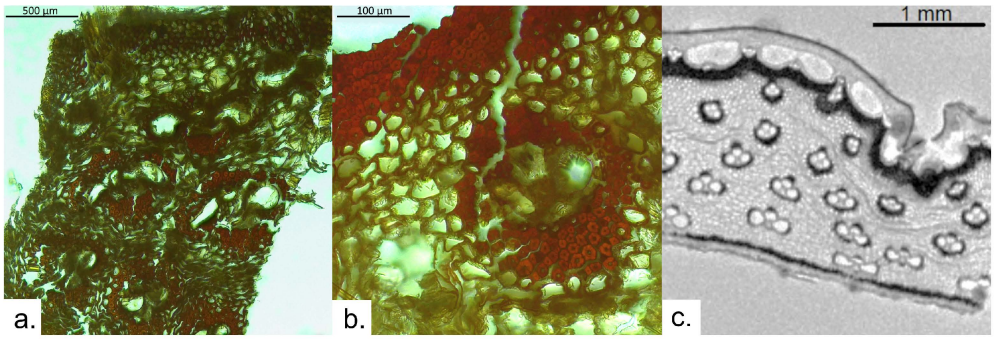

Figure 4. Archaeological reed fragment, preserved by desiccation, swept from the surfaces of the tomb of Tutankhamun in 1933 and preserved in a box in the Grand Egyptian Museum; (**a**) thin section observed via optical microscopy; (**b**) detail of vascular bundle observed via OM; and (**c**) µ-MRI image.

The MR image allows us to obtain an overall view of the archaeological sample (2 mm thick), starting from the outer layer (the epidermis) of medium thickness. This is characterized by black voxels due to the smaller lumen of its cells, which hinder water more than the subepidermal cells. The subepidermal tissue is followed by large longitudinal aerenchyma channels, whose function is to facilitate oxygen diffusion from the shoots to the root tips [33]. Going inwards, a dark layer of cortical sclerenchyma is observed. In this case, the darker color is due to the accumulation of paramagnetic substances, which likely indicates an advanced degradation of this area compared to the others. Three vascular bundles, composed of three large cavities each, are embedded in the cortical sclerenchyma. Four rows of vascular bundles of increasing size going inwards are also found in the cortex. These are wider than tall and have an average width of 300 µm. They comprise three large cavities each: two large metaxylem vessels and the protophloem. At least one smaller vessel can be observed in most vascular bundles. Vascular bundles are surrounded by bundle sheath sclerenchyma, which appears thicker going outwards. The overall density of vascular bundles is approximately 465 vascular bundles/cm^2. Finally, a thick black layer delimits the inner surface of the stem. The black line indicates dense non-porous tissue where water has not penetrated, with a possible presence of paramagnetic substances which, by producing a local inhomogeneity of the magnetic field, drastically reduce the signal intensity [34].

The μ-MRI images, obtained by virtually cutting the sample, allowed us to observe the whole reed fragment, retaining its diagnostic features. Thus, it was possible to identify the archaeological fragment as *Phragmites australis*. The identification was based on a series of factors, including the overall thickness of the sample (from the epidermis to the inner surface of the stem). Another feature was the clearly lined inner surface and rather thin sclerenchyma sheaths surrounding the vessels. Furthermore, vascular bundles appear wider than tall in the archaeological sample, as in the reference sample of *P. australis*. However, the most striking feature was the presence of large aerenchyma channels. These were not observed in either of the selected modern reference samples from the emerging part of reeds. Aerenchyma channels are completely absent in *Arundo donax* and present in submerged culms of *Phragmites australis* [35]. The presence of aerenchyma channels appears to be related to the water table level, as emerging parts appear to lack aerenchyma, which is evident in the waterlogged parts [36]. This difference can also be observed in samples analyzed by Kawasaki et al. [7]. This leads us to believe that the studied archaeological sample corresponds to a submerged reed part.

4. Discussion

The aim of this paper was to test the application of micro-magnetic resonance imaging for the examination of plant stems. To this end, we included a comparison of optical microscopy and μ-MRI, showing that the first technique attains a higher image resolution compared to the second, as already reported by Stagno et al. [25]. However, the image resolution in MRI is not strictly limited by the technique itself; instead, it depends on the instrumentation used, particularly the strength of magnetic gradients. In fact, spectrometers that feature more powerful magnetic gradients can achieve resolutions of approximately 1 μm [25]. Despite having a lower resolution compared to optical microscopy and scanning electron microscopy, the application of μ-MRI in this specific context, involving an archaeological mummified/desiccated sample, allowed us to obtain considerably clearer images of the studied archaeological specimen. While the obtained image retains a high resolution, the studied sample lost integrity upon being cut with a razor blade and could no longer be used for diagnostic purposes. This problem was not encountered with μ-MRI, as all the images were obtained by a virtual cut of the sample, allowing us to observe the whole reed fragment as well as retain its diagnostic features.

Although numerous parameters, such as the thickness of the cross-section, the shape and size of the vascular bundles, and the number of rows of vascular bundles in the cortex, were used for the identification of the archaeological sample, the presence of aerenchyma channels was a crucial diagnostic criterion. These channels are air-storing tissues at the rhizome periphery of *Phragmites australis*, typically rectangular in this species [35]. These are not present in *Arundo* species [35]. The existence of well-developed aerenchyma systems is a significant anatomical adaptation that facilitates the transfer of oxygen from aboveground organs to rhizomes and roots [37]. However, this type of structure is only present in the submerged parts of reeds [36]. It is for this reason that aerenchyma channels were not observed in the modern reference sample of *P. australis* investigated in this study.

When evaluating the proposed method, it is worth considering the necessity of soaking a sample for μ-MRI analysis. While this does not represent an issue for waterlogged archaeobotanical remains, this problem cannot be omitted when it comes to evaluating the advantages and disadvantages of applying μ-MRI for the study of desiccated and charred material. Compared to optical microscopy—which requires a fresh or soaked sample for the preparation of thin sections or even embedding in resin when detailing with particularly fragile or degraded plant material [38]—μ-MRI proves to be a less-invasive method. This technique, in fact, only requires soaking the sample and placing it in the NMR capillary tube. Images are then acquired by virtually orienting and slicing the specimen [25], avoiding manipulation and limiting the required sample size. On the other hand, variable pressure scanning electron microscopy (VP-SEM), which has been used in the past for the study of archaeological reeds (e.g., [23]) and is still the preferred method for non-invasive and

non-destructive analysis, has the advantage of not requiring sample preparation, including soaking [39]. However, it is preferable for observed wood/stem surfaces to be rather even, which can be achieved in different ways, such as fracturing charcoals [40] or preparing thin sections of waterlogged wood and treating them with albumin [41]. Another issue relates to sample size limitations, which are determined by the diameter of the NMR tube [25] or the VP-SEM chamber [39]. For this reason, when dealing with bigger samples (such as the ones subject of the present study), subsampling can prove to be necessary for all the discussed techniques. Nevertheless, it is important to highlight that sample size limitations are not dependent on either of the techniques but rather on the available instrument model [29].

5. Conclusions

In the present paper, we evaluated the application of μ-MRI for identifying archaeological reeds, which proved highly beneficial. In fact, in this specific case, it allowed us to clearly observe the transversal section of the studied sample, which, in contrast, disintegrated through cutting with a razor blade made to obtain a thin section for the conventional optical microscopy inspection. While μ-MRI requires soaking a sample in water, unless this is already preserved by waterlogging, it offers the advantage of providing a great variety of image contrasts associated with various chemical, physical, and physiological features. To obtain high-resolution MR images, other than high magnetic gradient strength, a small-bore magnet and a small field of view are required. Therefore, μ-MRI is suitable for analyzing small samples unless a larger-bore instrument, such as those used for the investigation of small animals, is employed. Therefore, it is possible to evaluate carrying this type of analysis on a subsample of the studied object. From a methodological perspective, this study introduces a novel application of nuclear magnetic resonance in the field of cultural heritage, which has the potential to be tested on a wider range of materials. Increasing the number of analytical approaches available for studying cultural heritage objects, with a focus on plant remains, will have several positive implications. Firstly, this has the potential to make scientific analyses more widespread and accessible, thus providing valuable information about numerous artifacts and contributing to the knowledge about plant exploitation by past communities. Secondly, this could represent an additional stimulus for technological development, which we are confident could lead to higher-resolution NMR images, further improving the quality of this type of analysis.

Author Contributions: C.M., V.S., N.M.H. and S.C.: conceptualization; C.M. and V.S.: data curation; V.S. and C.M.: formal analysis; N.M.H., S.C., L.S. and G.F.: funding acquisition; C.M., V.S. and S.C.: investigation; C.M., V.S. and S.C.: methodology; L.S. and S.C.: project administration; L.S., S.C. and N.M.H.: resources; L.S., G.F. and S.C.: supervision; C.M., V.S., N.M.H., L.S., G.F. and S.C.: validation; C.M., V.S. and S.C.: visualization; C.M., V.S. and N.M.H.: roles/writing—original draft; C.M., V.S., N.M.H., L.S., G.F. and S.C.: Writing—review and editing. All authors have read and agreed to the published version of the manuscript.

Funding: The analyses have been developed in the frame of two projects, "NMR analysis of Tutankhamun remains" of CNR ISC and a Sapienza University project, "Unraveling a mistery: the plant and organic remains from the Tutankhamon funerary set". This work was also supported by the Ministry of Foreign Affairs and International Cooperation (MAECI) in the form of a grant in favor of foreign citizens and Italian citizens living abroad (IRE).

Data Availability Statement: The data presented in this study are available in this article.

Acknowledgments: The authors are grateful to Elena Grossi for the linguistic revision that she carried out.

Conflicts of Interest: The authors declare no conflict of interest. The funders had no role in the design of the study, in the collection, analyses, or interpretation of data, in the writing of the manuscript, or in the decision to publish the results.

References

1. Liu, J.; Kopold, P.; van Aken, P.A.; Maier, J.; Yu, Y. Energy storage materials from nature through nanotechnology: A sustainable route from reed plants to a silicon anode for lithium-ion batteries. *Angew. Chem.* **2015**, *127*, 9768–9772. [CrossRef]
2. Enciclopedia Treccani. Canna. Enciclopedia Online. Available online: https://www.treccani.it/enciclopedia/canna#:~:text=Nome%20genericamente%20attribuito%20a%20numerose,che%20coniugano%20resistenza%20ed%20elasticit%C3%A0 (accessed on 10 September 2023).
3. Ramsey, M.N.; Maher, L.A.; Macdonald, D.A.; Nadel, D.; Rosen, A.M. Sheltered by reeds and settled on sedges: Construction and use of a twenty-thousand-year-old hut according to phytolith analysis from Kharaneh IV, Jordan. *J. Anthropol. Archaeol.* **2018**, *50*, 85–97. [CrossRef]
4. Oron, A.; Galili, E.; Hadas, G.; Klein, M. Early maritime activity on the Dead Sea: Bitumen harvesting and the possible use of reed watercraft. *J. Marit. Archaeol.* **2015**, *10*, 65–88. [CrossRef]
5. Romano, L.; Celant, A.; Montorfani, M.V. Reed-swamps in the Sumerian material culture: Archaeological, archaeobotanical, and experimental insights from the Abu Tbeirah excavations. In *Southern Iraq's Marshes: Their Environment and Conservation*; Jawad, L.A., Ed.; Springer: Cham, Switzerland, 2021; pp. 33–54.
6. Kolesik, P.; Mills, A.; Sedgley, M. Anatomical characteristics affecting the musical performance of clarinet reeds made from *Arundo donax* L. (Gramineae). *Ann. Bot.* **1998**, *81*, 151–155. [CrossRef]
7. Kawasaki, M.; Nobuchi, T.; Nakafushi, Y.; Nose, M.; Shiojiri, M. Structure and biomechanics of culms of *Phragmites australis* used for reeds of Japanese wind instrument "hichiriki". *Microsc. Res. Tech.* **2015**, *78*, 260–267. [CrossRef] [PubMed]
8. Perdue, R.E. *Arundo donax*—Source of musical reeds and industrial cellulose. *Econ. Bot.* **1958**, *12*, 368–404. [CrossRef]
9. Mercuri, A.M.; Sadori, L.; Blasi, C. Editorial: Archaeobotany for cultural landscape and human impact reconstructions. *Plant Biosyst.* **2010**, *144*, 860–864. [CrossRef]
10. Miksicek, C.H. Formation processes of the archaeobotanical record. *Adv. Archaeol. Method Theory* **1987**, *10*, 211–247.
11. Boulos, L.; Fahmy, A.G.E.D. Grasses in ancient Egypt. *Kew Bull.* **2007**, *62*, 507–511.
12. Noaman, S. Usage of *Arundo donax* L. as a sustainable material in interior design and architecture. In *Cities' Identity Through Architecture and Arts, Proceedings of the International Conference on Cities' Identity through Architecture and Arts (CITAA 2017), Cairo, Egypt, 11–13 May 2017*; Catalani, A., Nour, Z., Versaci, A., Hawkes, D., Bougdah, H., Sotoca, A., Ghoneem, M., Trapani, F., Eds.; Routledge: London, UK, 2018; p. 201.
13. Kiviat, E. What reed (*Phragmites*) ecology tells us about reed management. Part 1. Confronting reed's lurid reputation. *News Hudsonia* **2005**, *20*, 1–6.
14. Thomas, E. Terrestrial marsh and solar mat. *J. Egypt. Archaeol.* **1959**, *45*, 38–51. [CrossRef]
15. Barakat, H.N.; Aziz, A. *Guide to Plants of Ancient Egypt*; Bibliotheca Alexandrina: Alexandria, Egypt, 2010.
16. Malek, J.; Moffett, J.; Hutchison, S.; Miles, E.; Magee, D.; Rawlinson, K.; Tutankhamun: Anatomy of an Excavation. Carter Archives—Main Object List: 001–049. Available online: http://www.griffith.ox.ac.uk/gri/carter/HomePage.html#042 (accessed on 15 September 2023).
17. Abdrabou, A.; Abdallah, M.; Sultan, G.M.; Mostafa, M.; Bayoumi, H.; Magdy, R.; Abd El Kader, M.A.; Hamza, N.M.; Mamdouh, D.; Elsayed, H.M.; et al. Tutankhamun's polychrome wooden shawabtis: Preliminary investigation for pigments and gilding characterization and indirect dating of previous restorations by the combined use of imaging and spectroscopic techniques. *Open Archaeol.* **2022**, *8*, 30–54. [CrossRef]
18. Peruzzi, G.; Ciccola, A.; Bosi, A.; Serafini, I.; Negozio, M.; Hamza, N.M.; Moricca, C.; Sadori, L.; Favero, G.; Nigro, V.; et al. Applying Gel-Supported Liquid Extraction to Tutankhamun's Textiles for the Identification of Ancient Colorants: A Case Study. *Gels* **2023**, *9*, 514. [CrossRef] [PubMed]
19. Cutler, D.F.; Botha, C.E.J.; Stevenson, D.W. *Plant Anatomy: An Applied Approach*; Blackwell Publishing: Malden, MA, USA, 2008.
20. Tian, S.; Yang, R.; Pan, Z.; Su, X.; Li, S.; Wang, P.; Huang, X. Anisotropic reed-stem-derived hierarchical porous biochars supported paraffin wax for efficient solar-thermal energy conversion and storage. *J. Energy Storage* **2022**, *56*, 106153. [CrossRef]
21. Schweingruber, F.H. *Anatomy of European Woods*; Haupt: Stuttgart, Germany, 1990.
22. Martín-Seijo, M.; Teira-Brión, A.; Currás, A.; Rodríguez-Rellán, C. After the fire: The end of a house life-cycle at the Iron Age site of Nabás (North-western Iberia). *Veg. Hist. Archaeobot.* **2020**, *29*, 427–446. [CrossRef]
23. Figueiral, I.; Bouby, L.; Buffat, L.; Petitot, H.; Terral, J.F. Archaeobotany, vine growing, and wine producing in Roman Southern France: The site of Gasquinoy (Béziers, Hérault). *J. Archaeol. Sci.* **2010**, *37*, 139–149. [CrossRef]
24. Baruch, U. Identification of Charred Wood Remains from 'En Gedi. *Atiquot* **2005**, *49*, 43–48.
25. Stagno, V.; Moricca, C.; Sadori, L.; Dell'Aglio, E.; Reale, R.; Capuani, S. Evaluation of the efficacy of micro-Magnetic Resonance Imaging compared with light microscopy to investigate the anatomy of modern and ancient waterlogged wood. *Magn. Reson. Imaging* **2023**, *102*, 164–178. [CrossRef]
26. Callaghan, P.T. *Principles of Nuclear Magnetic Resonance Microscopy*; Oxford University Press Inc.: New York, NY, USA, 1991.
27. Cole-Hamilton, D.I.; Kaye, B.; Chudek, I.A.; Hunter, G. Nuclear magnetic resonance imaging of waterlogged wood. *Stud. Conserv.* **1995**, *40*, 41–50.
28. Telkki, V.V. Wood Characterization by NMR & MRI of Fluids. *eMagRes* **2012**, *1*, 215–222.
29. Longo, S.; Egizi, F.; Stagno, V.; Di Trani, M.G.; Marchelletta, G.; Gili, T.; Fazio, E.; Favero, G.; Capuani, S. A multi-parametric investigation on waterlogged wood using a magnetic resonance imaging clinical scanner. *Forests* **2023**, *14*, 276. [CrossRef]

30. Germer, R. *Die Pflanzenmaterialien aus dem grab des Tutanchamun*; Gerstenberg Verlag: Hildesheim, Germany, 1989.
31. El-Gawad, A.M.A.; El-Amier, Y.A. Anatomical features of three perennial swampy plants of Poaceae, grown on the water stream banks in Nile Delta, Egypt. *J. Med. Bot.* **2017**, *1*, 58–64. [CrossRef]
32. Spatz, H.C.; Beismann, H.; Brüchert, F.; Emanns, A.; Speck, T. Biomechanics of the giant reed *Arundo donax*. *Philos. Trans. R. Soc. London. Ser. B Biol. Sci.* **1997**, *352*, 1–10. [CrossRef]
33. Yamauchi, T.; Shimamura, S.; Nakazono, M.; Mochizuki, T. Aerenchyma formation in crop species: A review. *Field Crops Res.* **2013**, *152*, 8–16. [CrossRef]
34. Capuani, S.; Gambarini, G.; Guarnieri, R.; Di Pietro, G.; Testarelli, L.; Di Nardo, D. Nuclear magnetic resonance microimaging for the qualitative assessment of root canal treatment: An ex vivo preliminary study. *Diagnostics* **2021**, *11*, 1012. [CrossRef] [PubMed]
35. Danin, A.; Naenny, W. Contribution to the recognition of reeds by their rhizome anatomy. *Flora Mediterr.* **2008**, *18*, 385–392.
36. Armstrong, J.; Afreen-Zobayed, F.; Blyth, S.; Armstrong, W. *Phragmites australis*: Effects of shoot submergence on seedling growth and survival and radial oxygen loss from roots. *Aquat. Bot.* **1999**, *64*, 275–289. [CrossRef]
37. Fogli, S.; Marchesini, R.; Gerdol, R. Reed (*Phragmites australis*) decline in a brackish wetland in Italy. *Mar. Environ. Res.* **2002**, *53*, 465–479. [CrossRef]
38. Bleicher, N. An easy low-budget method to produce thin-sections of heavily decayed archaeological wood. *Dendrochronologia* **2008**, *26*, 9–11. [CrossRef]
39. Stokes, D.J. *Principles and Practice of Variable Pressure/Environmental Scanning Electron Microscopy (VP-ESEM)*; John Wiley and Sons: West Sussex, UK, 2008.
40. Cartwright, C.R. Identifying the woody resources of Diepkloof Rock Shelter (South Africa) using scanning electron microscopy of the MSA wood charcoal assemblages. *J. Archaeol. Sci.* **2013**, *40*, 3463–3474. [CrossRef]
41. Balzano, A.; Merela, M.; Čufar, K. Scanning electron microscopy protocol for studying anatomy of highly degraded waterlogged archaeological wood. *Forests* **2022**, *13*, 161. [CrossRef]

Disclaimer/Publisher's Note: The statements, opinions and data contained in all publications are solely those of the individual author(s) and contributor(s) and not of MDPI and/or the editor(s). MDPI and/or the editor(s) disclaim responsibility for any injury to people or property resulting from any ideas, methods, instructions or products referred to in the content.